Antimicrobial activity of GN peptides and their mode of action

Mojsoska, Biljana; Nielsen, Hanne Mørck; Jenssen, Håvard

Published in:
Biopolymers

DOI:
10.1002/bip.22796

Publication date:
2016

Document Version
Peer reviewed version

Citation for published version (APA):
Mojsoska, B., Nielsen, H. M., & Jenssen, H. (2016). Antimicrobial activity of GN peptides and their mode of action. *Biopolymers*, *106*(2), 172-183. https://doi.org/10.1002/bip.22796

Antimicrobial activity of GN peptides and their mode of action

Troels Godballe[1], Biljana Mojsoska[1], Hanne M. Nielsen[2], Håvard Jenssen[1,*]

[1]*Dept. of Science, Systems & Models, Roskilde University, Universitetsvej 1, DK-4000 Roskilde, Denmark.*

[2]*Dept. of Pharmacy, Biologics, University of Copenhagen, Universitetsparken 2, 2100 Copenhagen, Denmark.*

*Corresponding Author: *jenssen@ruc.dk* Tel +45 4674 2877

Abstract

Increasing prevalence of bacteria that carries resistance towards conventional antibiotics has prompted the investigation into new compounds for bacterial intervention to ensure efficient infection control in the future. One group of potential lead structures for antibiotics is antimicrobial peptides due to their characteristics as naturally derived compounds with antimicrobial activity. In this study we aimed at characterizing the mechanism of action of a small set of *in silico* optimized peptides. Following determination of peptide activity against *E. coli, S. aureus* and *P. aeruginosa,* toxicity was assessed revealing meaningful selectivity indexes for the majority of the peptides. Investigation of the peptides effect on bacteria demonstrated a rapid growth inhibition with signs of bacterial lysis together with increased bacterial size. Both visual and quantitative assays clearly demonstrated bacterial membrane disruption after 10 minutes for the most active peptides. The membrane disrupting effect was verified by measuring the release of calcein from bacterial mimicking liposomes. This revealed the most active peptides as inducers of immediate release, indicating the kinetics of membrane permeabilization as an important determinant of bacterial activity. No well-defined secondary structure of the peptides could be determined using CD-spectroscopy in the presence of different liposomes mixtures, implying that there is no correlation between peptide secondary structure and the observed anti-bacterial and cytotoxic activity for this set of peptides. In conjunction, these findings provide strong indications of membrane disruption as the primary mechanism of bacterial growth inhibition for the tested peptides.

Keywords: Antibacterial host defence peptides; Membrane destabilization, Antibacterial mode of action; Anti-infective; b

Introduction

For a long time, the treatment of most infections in western countries has been considered a rather uncomplicated matter due to the effectiveness of various antibiotics. Fortunately that still applies, although the treatment of some bacterial infections has become gradually more complicated in recent years because of the increase in bacterial resistance against conventional antibiotics. This is made obvious by the fact that infectious diseases are the third leading cause of death in developed countries, despite the abundant availability of antibiotics [1].

The emergence of bacteria with resistance towards conventional antibiotics is increasing at an alarming rate especially in hospital settings, seriously hampering effective treatment of infections [2]. Methicillin-resistant *Staphylococcus aureus* (MRSA) was in 2005 estimated to have caused 94 000 infections leading to 19 000 deaths [3] and together with other multi drug resistant (MDR) strains of *Pseudomonas aeruginosa* and extended-spectrum-beta-lactamase (ESBL) producing *Klebisella pneumonia* and *Escherichia coli,* they pose an increasing threat to public health [4]. On top of this there has only been introduced a very limited number of new antibacterial agents to the market since the 60's which together with a rapid declining interest from medical companies into development of new antibiotics, illustrates a development that calls for concern [2, 4]. In that perspective, it is important to pursue the development of new antimicrobial agents, with a novel mode of action, to ensure that we will be able to cure life-threatening infections in the future. One such group of compounds that has the potential to assist in the fight against infections is antimicrobial peptides.

Antimicrobial peptides are a natural component of the innate immune system in a wide range of organism, acting as a first line of defense against various microbes. These peptides have been isolated from a great number of organisms ranging from bacteria to plants, invertebrates and vertebrates, thereby demonstrating their prevalence in virtually all branches of life [5]. In relation to their abundance among different kinds of organisms, the biological effect varies from direct bacterial inhibition [5] to immune modulating [6], proving their versatility as effector molecules. The variety in origin and biological effect is reflected in the characteristics of antimicrobial peptides having a great deal of diversity, in both primary and secondary structure, probably explaining their evolutionary success [7]. Even so, there are a number of structural similarities that apply for most antimicrobial peptides, usually

being relatively short, ranging from 12-50 amino acids, carrying a net positive charge of +2 to +9 and having a distinct proportion of hydrophobic residues [8].

The positive charge of antimicrobial peptides is generally accepted as the main feature that mediates selectivity towards bacteria by harboring sufficient electrochemical attraction towards the negatively charged outer entities of bacterial cells to allow selective activity. As natural compounds with an antimicrobial effect, antimicrobial peptides have drawn the attention of scientist to investigate their potential as future antimicrobial agents. This has led to the identification of more than 1000 antimicrobial peptides [9], and numerous attempts to improve activity by modifying natural antimicrobial peptides or the *de novo* design of antimicrobial peptides [10] including the use of unnatural amino acid analogues [11]. Although a large number of natural and synthetic antimicrobial peptides have been studied, there are still today, questions tied to the exact nature of bacterial inhibition exerted by these peptides. Compiling evidence suggests that antimicrobial peptides have a plethora of effects against bacteria, ranging from unspecific membrane perforation to specific inhibition of intracellular targets and the bacterial inhibition exerted by some antimicrobial peptides is possibly the result of more than just one isolated mechanism [5]. Although different targets have been identified, a detailed characterization of the mode of action has only been carried out on a minority of peptides. To truly take advantage of antimicrobial peptides and make use of their potential as lead structures for bacterial intervention, it is therefore in that perspective that the scope of this work is to elucidate the mechanism of action of a set of different synthetic antimicrobial peptides. The antimicrobial peptides used in this study were originally designed by Fjell and colleagues by the use of *in silico* screening [12]. The 10 most active peptides from this optimization were selected for investigation in this study, all having a positive charge of +4, uniform chain length of 9 amino acids and at least three tryptophan residues. To verify the activity of the peptides, minimal inhibitory concentration (MIC) testing was carried out against *E. coli, P. aeruginosa and S. aureus* reference strains and the two most active peptides were selected for further studies to elucidate the mechanism of bacterial inhibition. Herein we demonstrate compelling evidence for membrane perforation as the main contributor of bacterial inhibition together with reversible metabolic disturbance at lower concentrations.

Material and methods

Solid phase peptide synthesis

The peptides were synthesized using solid phase Fmoc chemistry with amidation on the carboxyl end, purified by reverse-phase HPLC using a C_{18} column (Higgins Analytical Inc. 10 μm 250x10 mm) and a water/acetonitile gradient. The correct mass and purity >95% was verified using Dionex Ultimate 3000 RP-UHPLC (C18 Kinetex 100 x 2.1 mm, 100 Å) electrospray ionization mass spectrometry (Finnigan LTQ) (**Figure S1, Table S1**).

Minimal inhibitory concentration determination

The antimicrobial efficacy of peptides was tested using a serial dilution titration, as previously described [13] on a panel of clinically relevant bacterial strains; i.e. *E. coli* (ATCC 25922), *P. aeruginosa* PAO1 (ATCC 15692), *S. aureus* (ATCC 29213). Conventional antibiotics used throughout the study include Ampicillin (A9518), Ciprofloxacin (17850), Tetracycline (T7660), Tobramycin (T4014) and Polymyxin B (92301), all purchased from Sigma. In short, overnight cultures were grown to mid-log phase before diluting to ~5×10^5 CFU/mL in Mueller Hinton broth (Becton Dickinson) and 90 μL was used to inoculate each well of a 96-well polypropylene plate (Cat. No. 3879, COSTAR). Then, 10 μL aliquots of a 2-fold dilution series of the peptides were added and the minimal inhibitory concentration (MIC) was scored as the lowest concentration that inhibited visible growth after 48 hours of incubation at 37°C.

Hemolysis assay

Freshly drawn human blood with EDTA as anticoagulant was washed and centrifuged at 500 g for 5 minutes until the appearance of clear supernatant. A two-fold dilution series of peptides was added to 96-well polypropylene microtiter plates (COSTAR Cat. No.3879) in 75 μL aliquots together with 50 μL of 4 % final concentration of red blood cells (RBC) giving a total volume of 125 μL. The plate was incubated with shaking for 1 hour at 37°C, before being centrifuged at 250 g for 5 minutes. 50 μL of the supernatant was diluted 1:3 in sterile saline in a flat bottomed 96-well greiner plate before

measuring absorbance at 414 nm, using a multi-detection microplate reader Synergy HT. 100 % lysis was defined as RBC treated with 1% Triton-X 100 and sterile saline treated RBC was added for baseline adjustments. The test range was 3.1-400 µg/mL.

MTT assay

Toxicity against HeLa cells was estimated by the MTT viability assay. HeLa cells were cultured in DMEM Glutamax media (32430-027, Invitrogen), media supplemented with 10% FBS and 1% pen/strep using standard techniques. The cells were passaged at least 2 times before being used in the assay, to ensure logarithmic growth. At 80 % confluency, cells were harvested, quantified and 10.000 cells/well were seeded in a 96-well microtitter plate. The cells were placed in a humidified 5% CO_2 atmosphere at 37°C for 24 hours. Media was aspirated and the cells were washed with PBS w/o Ca^{2+} and Mg^{2+}. A mixture of peptide and DMEM media (100 µl) was added and the cells were incubated in a humidified 5% CO_2 atmosphere at 37°C for 1 hour before wash with PBS with or without Ca^{2+} and Mg^{2+}. MTT (50 µg) dissolved in PBS with or without Ca^{2+} and Mg^{2+} was added and the cells were incubated 90 minutes in a humidified 5% CO_2 atmosphere at 37°C. MTT solution was aspirated and 100 µL of DMSO was added to dissolve the formazan crystals before incubating 5 minutes at 37°C. The absorbance at 540 nm was read in a multi-detection microplate reader Synergy HT. Viability control was assigned to samples with only HeLa cells and DMEM media and 0 % viability was assigned to samples with 1 % added Triton-X-100 instead of peptides. The assay was done 3 times with duplicates and results are the mean of these. Concentrations giving a 50% reduction in metabolism (IC_{50}), was calculated using equation (I) in Graphpad Prism.

$$Y = \frac{100}{1+10^{((LogIC50 \div X)\cdot HillSlope)}} \qquad \text{(Eq. I)}$$

Killing kinetics

Colony forming units (CFU) counts were monitored for 180 minutes, following peptide exposure at concentration corresponding to 1×, 2× and 4×MIC. Overnight culture of *E. coli* ATCC 25922 was diluted with fresh Mueller Hinton broth and re-grown to mid-log phase before diluting to a turbidity of OD_{600} 0.1 and loading 90 µL into wells of a flat bottomed 96-well Greiner plate containing 10 µL of peptides solution. Growth control was assigned to wells without peptide. The content of individual plates was collected and plated out in duplicate on LB agar plates. Between extractions, the microtitter plate was sealed and placed at 37°C. LB agar plates were incubated for 18 hours at 30°C and colonies were counted. The presented results are the mean of 3 independent experiments.

The effect of peptides on bacterial growth was investigated by monitoring optical density (OD) following peptide exposure. Overnight culture of *E. coli* ATCC 25922 was diluted with fresh Mueller Hinton broth and re-grown to mid-log phase before diluting to a turbidity of OD_{600} 0.1. A microtiter plate was filled with 10 µL of peptide or antibiotic solution per wells, before loading 90 µL of bacterial suspension. For both peptides and antibiotics, concentrations corresponding to 1×-, 2×- and 4×MIC were used. OD_{600} was measured, with a multi-detection microplate reader Synergy HT at 37°C, every 8 minutes for 5 hours with shaking. The readings were baseline corrected against wells with only Mueller Hinton broth. Comparison between a standard spectrophotometer, with a cuvette length of 1 cm, and the readings obtained from the plate reader showed a difference with 5-fold lower readings from the plate reader (data not shown). In order to make readings meaningful, in relation to the correlation between optical density and concentration of bacterial cells, the readings from the plate reader was multiplied with a factor of 5.

The effect on both bacterial DNA content and change in cell size after exposure with peptides was monitored over 180 minutes by flow cytometry. An overnight culture of *E. coli* ATCC 25922 was diluted with fresh Mueller Hinton broth and re-grown to mid-log phase before diluting to a turbidity of OD_{600} 0.1. A total of 90 µL of this bacterial suspension was loaded into a flat bottomed 96-well Greiner plate for peptide and antibiotic samples and 100 µL for control samples. After extraction of the zero sample, 10 µL of peptide solution corresponding to 1× and 4× the MIC concentration was added for a total volume of 100 µL. Two wells were loaded for each treatment to ensure enough bacteria for the

flow cytometry analysis. Immediately after extraction the samples were put on ice and centrifuged at 10 000 g for 5 minutes at 4°C and resuspended in 100 µL 10 mM Tris HCl pH 7.4 before fixing with 1000 µL 77% ethanol. The following day, the samples were centrifuged at 10 000 g for 5 minutes before gently removing the supernatant and adding 140 µL staining solution (90 µg/mL Mitramycin and 20 µg/mL ethidium bromide in 10 mM Tris pH 7.4, 10 mM $MgCl_2$). The samples where run on an A10 Bryte Flow Cytometer and when possible, 20 000 events were included in the analysis.

Membrane depolarization assay

The LIVE/DEAD® BacLight ™ Bacterial Viability Kit (L7012, Invitrogen), was applied to peptide treated *E. coli* ATCC 25922, to investigate a visual indication of the membrane permeability capabilities of the peptides. Overnight culture of *E. coli* ATCC 25922 was diluted with fresh Mueller Hinton broth and re-grown to mid-log phase before diluting to a turbidity of OD_{600} 0.1. Then 10 µL of peptide solution corresponding to a final test concentration of 1× and 4×MIC was added to a flat bottomed polystyrene Greiner plate before loading 90 µL of bacteria suspension. 100 µL of bacterial suspension was used as a control. Each well corresponded to one time point for each individual treatment. The plate was placed at 37°C and the samples were extracted at the indicated time points and immediately put on ice. The samples were then centrifuged at 10 000g for 5 minutes, and the pellet resuspended in 100 µL 0.9% ice cold NaCl, to remove interfering media components. Staining solution (1 µL) was added and incubated for 15 minutes in the dark, before loading to 1% agarose slips on microscope slides. Staining solution was prepared by adding 5 µL of 3.3 mM Syto-9 dye in DMSO (Compound A) and 5 µL of 20 mM Propidium iodide in DMSO (Compound B) to 20 µL of sterile water. Samples were inspected with a Leica DM5000B microscope using a mercury lamp. A filter cube with excitation filters of 436, 495 and 580 nm and emission filters of 460, 535 and 630 nm was used to be able to detect both live and dead bacteria.

To verify the findings from microscope pictures with an assay that could characterize the membrane permeability of the entire bacterial population in the samples, the Live/Dead quantification was performed. The assay was essentially performed according to the manufacturer's instructions. After establishing a standard curve from known ratios of isopopyl killed and live bacteria an overnight

culture of *E. coli* ATCC 25922 was diluted with fresh Mueller Hinton broth and re-grown to mid-log phase before diluting to a turbidity of OD_{600} 0.1. The bacterial solution and peptide solution was mixed in a 9:1 ratio (vol/vol) in a 96-well polypropylene plate (Cat. No. 3879, COSTAR) and incubated at 37°C. At the indicated timepoints the content of individual wells was extracted, put on ice and then pelleted at 11 000 g for 8 minutes before being resuspended in 0.9% NaCl and placed on ice again. The resuspended bacterial suspension was then added to individual wells of flat bottomed 96-well polystyrene plate and mixed with 100 µL staining solution before incubation in the dark for 15 minutes and subsequent measurement of fluorescence on a multi-detection microplate reader Synergy HT. Green fluorescence was excited at 485 nm and the emission detected at 528 nm, whereas the red fluorescence was excited at 530 nm and detected at 645 nm. Percentage of living cells was obtained by using equation (II) using the standard curve made from known ratios of live cells. The staining solution was prepared by adding 3 µL of both compound A and B, for each 1 mL of distilled sterilized water and stored in the dark.

$$\%\ live\ cells = \frac{Green\ fluorescence}{Red\ fluorescence} \bullet \frac{1}{0.0627} \qquad \text{(Eq. II)}$$

Liposome preparation

Large unilamellar vesicles (LUVs) was prepared by mixing POPC (1-palmitoyl-2-oleoyl-sn-glycero-3-phosphocholine) and POPG (1-palmitoyl-2-oleoyl-sn-glycero-3-phosphoglycerol) and in a molar ratio of 3:7 as a simple mimic of bacterial membranes and POPC:POPG:Cholesterol was mixed in a molar ratio of 5:2:3 as a simple mimic of mammalian membrane. POPC (770557), POPG (770257) and Cholesterol were all purchased from Avanti Lipids (Alabaster, Alabama). The lipid mixture was concentrated on a rotary evaporator and washed 3 times with 99.9 % ethanol to remove residual organic solvents. The lipid mixture was then dissolved in 4 mL HEPES buffer (10 mM HEPES, 150 mM KCl, 0.03 mM $CaCl_2$, 0.01 mM EDTA, pH 7.4) with 20 mM calcein (C0875, Sigma), for calcein containing liposomes and 10 mM Tris pH 7.4 for empty liposomes used for CD spectroscopy, followed by thorough mixing and sonication for 5 minutes to prevent aggregates. Subsequently, the lipid mixture was vigorously whirlmixed every 10 minutes over the course of 1 hour and finally left at room temperature for 1 hour, to allow the lipids to anneal. LUVs were prepared by extruding the lipid

mixture through, two double stacked 100 nm filters, a total of 10 times using a Nitrogen powered extruder. The calcein containing liposomes were loaded on Sephadex G-50 columns to separate encapsulated calcein from free calcein and eluted with HEPES buffer. The size of the liposomes was verified to be approximately 110 nm with a narrow size distribution by dynamic light scattering (DLS) using a Zetasizer Nano ZS (Malvern, Worcestershire, UK). Malvern DTS v. 5.10 software (Malvern, Worcestershire, UK) was used for acquisition and analysis. By comparing the end volume with the starting volume, the dilution of the initial liposome concentration was estimated and that lead to the anticipation of a stock concentration of 971 μM of the liposomes.

Calcein release assay

Calcein release was done in a 96-well plate with shielded wells (MicroWell 96 optical bottom plate, NUNC, Roskilde, DK). 100 μL of peptide diluted in 10 mM HEPES buffer was added and immediately before measurement of leakage, 80 μL of 45 μM liposome suspension was added for a final liposome concentration of 20 μM. The liposome concentration was calculated from the starting concentrations of lipids, taking into account the change in volume during preparation, and assuming a 100% yield from the sephadex column. Measurements were performed in a FLUOstar OPTIMA plate reader at an excitation wavelength of 485 nm and an emission wavelength of 520 nm over the course of 1 hour at 37°C. Maximum leakage of liposomes was acquired by lysis with 10% Triton and release following peptide exposure, was calculated using equation (III), where F_{max} denotes fluorescence after addition of 10% Triton, F_0 represents background fluorescence of liposomes and F designates the fluorescence intensity after peptide addition.

$$\%\ leakage = 100 \bullet \left(\frac{F - F_0}{F_{\max} - F_0} \right) \qquad \text{(Eq. III)}$$

Results

This study aimed at characterizing the bacterial inhibition and antibacterial mode of action of a set of highly active antimicrobial peptides earlier identified by Fjell *et al.* [12]. The GN peptide library was screened for antibacterial activity against Gram-negative *E. coli* ATCC 25922 and *P. aeruginosa* ATCC PAO1 and Gram-positive *S. aureus* ATCC 29213 bacteria. The minimal inhibitory concentrations of the tested peptides demonstrated a significant spread in activity pattern from 1.5 to 100 μg/mL (**Table 1**). Potent broad spectrum activity against both Gram-negative and Gram-positive bacteria was observed for GN-2, GN-4 and GN-6 peptides. For specific activity against *E. coli*, GN-14 exhibits as good antimicrobial activity as GN-2, GN-4 and GN-6 peptides. Similarly, a pronounced antimicrobial activity against *S. aureus* was observed for GN-5 peptide (1.5 μg/mL), and GN-2 and GN-6 peptides (3.1 μg/mL). However, in respect to a broad spectrum antimicrobial potential, peptide GN-2 and GN-4 appear as best candidates.

In an attempt to explain the antibacterial peptide properties with classical chemical properties the hydrophobic moment was measured for all the peptides. This quantitative measure of the peptides amphipathicity indicates that antibacterial activity increases proportionally with the hydrophobic moment (**Table 1**). In order to further characterize the antimicrobial profiles of the GN peptides, their ability to selectively target bacterial- versus mammalian cells was assessed using hemolytic assay. Human red blood cells were exposed to different concentrations of GN peptides and the degree of lysis was evaluated. All peptides resulted in a dose dependent release of hemoglobin, and toxicity is reported as the highest concentration of peptides resulting in less than 10 % lysis compared to PBS treated control cells (**Table 1**). Comparing antibacterial and hemolytic potential, the peptide library clearly separates into two sub-groups; GN-8, -9, -11 and -12 being hardly hemolytic with low antimicrobial potential, while the remaining peptides demonstrate an overall higher antibacterial effect yet still only modest hemolytic activity. Thus, for this set of peptides the tendency to lyse human red blood cells is highly correlated with the ability to kill bacteria. In comparison, indolicidin, a small 13 amino acids tryptophan and arginine rich antimicrobial peptide[14], is used as an antibacterialreference peptide indicating that most of the GN peptides have superior selectivity. To further complement the assessment of the potential toxicity of the GN peptides, a MTT assay was performed on HeLa cells and the inhibitory concentrations giving 50 % reduction (IC_{50}) of cellular metabolic activity were calculated

(**Table 1**). The results are in agreement with the hemolytic activity, thus demonstrating that the peptides with the highest antimicrobial activities are the peptides exhibiting the greatest metabolic inhibition in HeLa cells. Hence, peptides GN-2 and GN-4 stand out as most cytotoxic with IC_{50} values of 47 and 37 μg/mL, respectively.

To dissect the antimicrobial activity of GN peptides with a range of different assays, GN-2 was chosen as the most potent peptide with good selectivity index range of 16 to 32. Correspondingly, GN-6 which structurally differs from GN-2 peptide in the presence of phenylalanine and a patch of 4 consecutive tryptophan residues was also considered for characterization for the mechanism of bacterial inhibition.

First to differentiate between bactericidal or bacteriostatic mode of antibacterial activity, colony forming unit counts were monitored for *E. coli* cultures exposed to 1×, 2×, and 4×MIC concentrations of GN-2 and GN-6 peptide. This assay illustrated the ability of the different peptide concentrations to reduce the colony forming unit counts over a period of 180 minutes. The GN-2 peptide demonstrates fast antimicrobial activity indicated by a decrease of exponentially growing bacteria within the first 40 minutes of exposure (**Figure 1**). The inhibition proceeds for 80 minutes after which there is a reestablished bacterial growth observed. Similar pattern is observed for GN-6 peptide with a slightly delayed inhibition. Bacterial inhibition is concentration dependent for both peptides, even though the standard error bars for GN-6 peptide at 4×MIC show high experimental variation.

To further elucidate the bacterial inhibition exploited by the peptides, bacterial mass was monitored by optical density readings at 600 nm over a course of 5 hours. The control bacteria display exponential growth until 120 minutes after which clear decrease in optical density is observed. There is a reestablished growth after 180 minutes, indicating that the decrease after 2 hours is not due to limited nutrition and/or waste build-up (**Figure 2**). A number of antibiotics were analyzed in parallel for growth inhibition patters so that the potential bacterial targets of GN-2 and GN-6 peptides could be elucidated. In addition to the viability experiments of exponentially growing *E. coli*, the optical density measurements revealed clear concentration dependent inhibition of the optical density readings when bacteria were exposed to 1×MIC concentration of both GN-2 and GN-6 peptide when compared to the untreated bacteria. The inhibition is most pronounced at 2×MIC concentration for both peptides. With respect to 1×MIC concentration of both peptides, the inhibition pattern is different indicating distinct

ways of exerting antimicrobial activity halting bacterial growth. Both peptides at 2×MIC concentration demonstrate low OD measurements indicative of some degree of bacterial lysis.

Flow cytometry analyses were used to characterize the effect of GN-2 and GN-6 peptide on cell size and DNA content. Exponentially growing *E. coli* were exposed to 1× and 4×MIC concentrations of GN-2 and GN-6 peptides and samples were analyzed every 20 minutes over a course of 3 hours for DNA content per cell mass extrapolated by fluorescence/lightscatter measurements. Untreated *E. coli* show fairly constant ratio of DNA per cell size indicative for a healthy growing bacterial population. Exposure to 1× and 4×MIC concentration of GN-2 gives pronounced initial decrease of DNA content per cell size as compared with the control samples. After 40 minutes of exposure an increase of DNA per cell size is observed for samples treated with 4×MIC concentration, referring to the reestablishing of the DNA content at this point. At 120 minutes the effect of DNA content per cell size follows similar ratio to that of the control, indicating a possible recovery (**Figure 3A**). Similar fashion of initial fast and persistent decrease of DNA per cell size followed by an increase after 40 minutes is observed for bacteria treated with 1×MIC concentration of GN-6 peptide.

The increase in cell size indicated by the lightscatter measurements observed in the flow cytometry data (**Figure S2**) is supported by the microscopy images taken at time zero and 180 minutes for the control *E. coli* population. Bacteria treated with GN-2 peptide at 1× and 4×MIC concentration appear slightly bigger in size than the control bacteria. Clear difference between cells treated with 1× and 4×MIC concentrations of GN-2 peptide is observed by the large areas of cell debris and bacteria transparency indicating cell lysis in samples treated with 4×MIC (**Figure 3C**). Upon treatment with GN-6 peptide at 4×MIC concentrations, there is a clear morphological change presented by cells that appear long and filamentous but not lysed (**Figure 3C**). This data is in agreement with the observations from the flow cytometry analyzes on DNA, size and DNA /size.

Live/dead staining experiments with SYTO9 green-fluorescent nucleic acid stain and propidium iodide red-fluorescent stain, were used to analyze the membrane permeability capacity of GN-2. Under conditions where no membrane permeabilizing agent is present, bacteria with intact membranes will stain green (**Figure 4A**). The un-treated control cells are naturally predominantly staining green at all time-points, illustrating a healthy population of bacteria. *E. coli* exposed to GN-2 peptide at 1×MIC

concentration at the 10 and 20 minutes time-point, demonstrate about 90 % permeabilized membranes, thus staining red. However, over time the surviving cells are replicating, resulting in an increasing percentage of green cells in the later time points (**Figure 4B**). Upon increasing the GN-2 peptide concentration to 4×MIC, the membrane integrity stays disrupted throughout the assay of 120 minutes (**Figure 4C**). To quantify the membrane permeability in a more un-biased fashion than microscopy, the same bacterial cultures were also analyzed using a multi-detection fluorescence plate reader. Plotting the ratio of live and dead cells for cultures incubated with 1×, 2× and 4×MIC concentration of GN-2 peptide over time, clearly demonstrates how 2× and 4×MIC knocks down the viability to around 20% and this level is kept for 120 minutes. Contrary, at 1×MIC of GN-2, the level of viable bacteria after 10 minutes is about the same as in the samples treated with 2× and 4×MIC of GN-2, but at 1×MIC the culture re-growths with a doubling time of about 1 hour (**Figure 4D**).

Due to previously established observation of membrane disruption as a primary mode of action of the GN peptides, calcein leakage assay was performed. This assay allows characterization of peptides based on the different potencies to provoke membrane leakage of calcein entrapped unilamellar phospholipid vesicles (LUVs) made of POPC:POPG (3:7 molar ratio). Calcein is a self-quenching molecule that at high concentration shows relatively low background fluorescence. As calcein molecules are being released to the exterior of the vesicles, the fluorescence increases. The percentage of calcein leakage can be plotted as a function of the concentration of the peptides. All GN peptides were able to induce calcein leakage in a concentration dependent manner at endpoint reading of 60 min (**Figure 5A**). But the release of calcein is much less significant that what is induced by melittin, a well-known peptide with non-selective lytic properties, used as a positive control for giving distinct pattern of liposome disruption [15].

As it was impossible to distinguish the lytic potential of the different GN peptides using an endpoint reading the release of calcein over time was monitored, enabling us to extract information about the capability of the peptides to induce calcein leakage. The GN-2 peptide demonstrates distinct kinetics of rapidly provoking calcein release from the liposomes, particularly at high concentrations (**Figure 5B**). Only a small concentration change from 3.5 μg/mL to 5.5 μg/mL of GN-2, changes the calcein release from about 30% to 100%. Conversely, the GN-6 peptide, which has slightly lower antimicrobial activity than GN-2, exerts a much more gradual release of calcein over time, which stabilizes after

about 10 minutes (**Figure 5C**). The gradual release is observed for a wider range of concentrations, suggesting different mode of membrane activity or different modes of action for this peptide compared to GN-2. This could potentially be reconfirmed and better characterized using the experimental design of Russel *et al.* 2010 [16]. A similar, but even more dramatic profile for gradual release is observed for GN-14 where gradual increase in calcein leakage progressing over a course of 20 minutes is observed (**Figure 5D**). The different patterns of calcein leakage attribute to the correlation of antimicrobial peptide activity and their ability to disrupt bacterial membranes, where more active peptides cause more instantaneous release of calcein from the liposome.

The secondary structure of GN peptides and melittin was inspected with circular dichroism (CD) spectroscopy to see whether or not a confined structure is necessary for the antimicrobial, toxic or membrane disrupting activities observed. Peptide secondary structures were measured in Tris buffer pH 7.4 and unilamellar phospholipid vesicles consisting of POPC:POPG:Cholesterol (5:2:3 molar ratio) and POPC:POPG (3:7 molar ratio), the latter mimicking mammalian and bacterial membranes, respectively (**Figure S3**). None of the peptides demonstrated any defined secondary structures in Tris buffer, indicating random coils under these conditions. In presence of LUV that mimic mammalian membranes, the control peptide melittin adopts a structural confirmation similar to that of an α-helix with peak minima at 222 and 208 nm [17]. Using the DichroWeb K2D algorithm [18], the α-helix content in melittin was calculated to be 77 % which is in agreement with other publications [19]. The CD spectra for the GN peptides are similar for mammalian and bacterial membrane mimics and illustrate no well-defined secondary structure in either environment. Therefore, it is reasonable to assume that GN peptides exert their antimicrobial, toxic and membrane disrupting activity without adapting any well-defined secondary structure.

Discussion

Due to the increased number of infectious agents that are resistant to many well-known classes of antibiotics, there is a constant need of improved alternative drug classes and therapies. In this study we present evaluation of the antimicrobial potencies of ten different peptides, GN-2 to GN-14, from the *in silico* optimized peptide library previously reported on by Fjell *et al.* [12]. These peptides are rich in tryptophan residues along with lysine and arginine in various orders along the backbone (**Table 1**). The contribution of the arginine, lysine and tryptophan residues to the antimicrobial activity is exerted by primary interaction of the charged residues with the net negative charge distributed on the surface of the bacterial membranes followed by insertion of tryptophan residues in the interfacial region of the phospholipid bilayer [20]. Beneficial features within the GN peptide library that exhibit somewhat higher antimicrobial activity than others are the cationic and bulky three residues in the amino terminal with specific annotation to the cationic residues which mediate interaction with the anionic lipids and lead to membrane instability in Gram-negative bacteria models [21]. This observation is further supported with the GN peptides -8, -9, -11 and -14 which have either leucine or isoleucine in addition to one cationic (either lysine or arginine) and one tryptophan residues within their structure and exhibit lower antimicrobial activities.

To understand the overall activity of the GN peptides and their ability to selectively discriminate between bacterial and mammalian membranes, and therefore obtain a selectivity index as a ranking tool for the most potential peptide candidate, hemolytic and toxic effects were investigated. A strong relationship between hydrophobicity and high antimicrobial activity and high toxicity has been reported in the literature[22]. Such observation could not be observed in this study for the GN peptides. GN-2 and GN-4 are the most active against both Gram-positive and Gram-negative bacteria and have both high hemolytic profiles. They share the same charge distribution along their backbone differing only in isoleucine (GN-2) and leucine (GN-4) at the C-terminal end and arginine (GN-2) and lysine (GN-4) at the 4^{th} position. The last feature suggests that the lysine residue in GN-4 peptide, which is previously ascribed as a contributor to the higher lytic effects [21], exerts the same effect when compared to arginine in GN-2 peptide (**Table 1**).

For a better differentiation of host cell toxicity, metabolic activities in HeLa cells were also monitored. Comparing toxicity against HeLa cells with the hemolytic properties of the GN peptides, reveals a disproportionally high toxicity towards the former (**Table 1**). This could be related to the peptides exerting higher selectivity to the more anionic cancer cells, similar to previous observations [23]. In addition, peptides that successfully entered HeLa cells could target intracellular membranes that resemble bacterial membrane such is the mitochondrial membrane and therefore inhibit metabolism that could be lethal to eukaryotic cells [24]. To further elucidate the observed toxicity of GN-2 and GN-4, peptides toxicity measurements on a non-cancerous mammalian cells or animal studies should be employed.

The current study demonstrate a fast decrease of exponentially growing *E. coli* when exposed to sub-MIC concentrations of both peptide GN-2 and GN-6 (**Figure 1 and 2**). The observed decrease is probably due to metabolic disturbance that halts bacterial growth for about 80 minutes, after which the growth is reestablished. This is also in agreement with the OD measurements, which revealed similar decrease in the bacteria growth under the same conditions. Flow cytometry analysis show that over a period of 80 minutes the cell size at MIC concentrations does not change significantly, thus supporting the above stated evidence (**Figure S2**). In support of this, the microscopic images reveal no obvious morphological difference except that the MIC treated samples appear slightly bigger in size. The increase in cell size is a result of metabolic inhibition which delays the decrease in cell size which is normally observed when bacterial suspension gets denser [25]. In contrast to the bacteriostatic inhibition at MIC concentration of both the GN-2 and GN-6 peptide, bactericidal inhibition is observed at 4×MIC concentrations. Inhibition through bacterial lysis is ascribed to GN-2 peptide which causes decrease in OD of *E. coli* over time, and such relationship has also been described in the literature [26]. The mechanism behind the bactericidal killing for GN-6 demonstrates no signs of lysis rather than filamentation which are reported as an increase in the lightscatter from the flow cytometry analysis [27]. These results are further corroborated by the microscopy studies. Prior studies have shown that the SOS response to ciprofloxacin and beta-lactams is ascribed to filamentation [28]and the same can be induced by multiple environmental stresses [29].

Disturbed membrane integrity of *E. coli* is observed after 10-20 minutes of exposure of 1×MIC concentration of GN-2 peptide, followed by gradual reestablishment or growth of cells that survived

the initial attack (**Figure 4**). The latter seems plausible as cells surviving exposure to the peptide would be in a rough and rather hostile environment, thus explaining their very slow growth. The phenomena observed between 40 and 80 minutes, does also correlates with the observations of constant cell size from flow cytometry analysis and a standstill in CFU. However, using live/dead staining analysis the reestablishment of membrane integrity has been ascribed to membrane reassembly which leads to propidium iodide exclusion [30] or possible efflux pumps that drive propidium iodide out of the cell [31]. The later mechanism would require presence of ATP for efflux pumps which could be in agreement with membrane leakage and escape of ions upon peptides acting on membranes at low concentrations, provoking ATP production [32]. In summary, it may seem as GN-2 induce sufficient membrane permeabilization for the entry of propidium iodine, but the process does not translate into full loss of viability. In relation to this observation, prior studies have shown that Bac8c, a peptide with sticking resemblance to the GN peptides, can causes membrane depolarization after 5 minutes of exposure followed by membrane recovery after 90 minutes [33]. In case of 2× and 4×MIC concentrations of GN-2 peptide, the peptide consistently causes membrane leakage supported by the visual and quantitative membrane leakage assays supported by CFU counts that show loss of bacterial viability (**Figure 3 and 4**).

The GN-2 peptide with a very narrow concentration range from 5.5 to 1.7 μg/mL induced instant release of calcein from model membranes, corresponding to 100% and 5%, respectively (**Figure 5**). This observation coincides with a proposed model of membrane active antimicrobial peptides binding to the surface of the phospholipids parallel to the membrane (S-state) and upon reaching a threshold change their orientation into perpendicular position (I-state), thereby inducing a more profound membrane disruption [32]. The GN-14 peptide revealed a more gradual release of calcein content which progresses over a period of 20 minutes. Such release has been ascribed to a mechanism of transient pore formation [34]where liposomes re-stabilize resulting in plateau state of calcein release [34-35], leaving partially depleted liposomes. Given that the GN peptides only are composed of 9 amino acids, the toroidal pore model is the more plausible mechanism of membrane action due to the fact that the pores in this model are stabilized by both lipids and peptides rather than only peptides as in the barrel-stave model [34]. A membrane mechanism involving toroidal pores are further supported by the lack of well

defined secondary structures in the GN peptide library (**Figure S3**), and none helical peptides have also by others been demonstrated to work through this mechanism [36].

Previous studies have shown that melittin is a pore forming membrane active peptide that acts in an all or none manner [19c, 37], resulting in these immediate release profiles of calcein. Since the current study showed similar kinetics in mediating calcein release for both melittin and GN-2, it is reasonable to assume that the GN-2 peptide also acts by pore formation mechanism. However the calcein release for mellitin is much more pronounced at lower concentrations when compared to the release for peptide GN-2 Fig.5A. Having said that it is important to stress out that melittin and GN-2 act with different potencies of 16.3 (3.5 μg/mL) lipid/peptide molar ratio for melittin and 5.4 (5.5 μg/mL) for the GN-2 peptide. Furthermore, we would argue that GN-6 which results in a much more gradual release of calcein, also could work through pore formation. The difference in kinetics of these peptides (GN-2 and GN-6) might be related to the lifetime of the pores [35, 38], the size of the pores and the number of pores [38], all of which reflects on the release of the entrapped molecules from the LUVs. Even though pore formation may seem the best mechanism of action of tested GN peptides, the possibility of membrane disruption exploited by a mixture of different mechanism should not be excluded [39]. The release of calcein for both peptides, GN-2 and GN-6, levels off over time (Figure 5B-C) and this type of behavior has been reported to indicate transient pore formation during the initial insertion step into the lipid bilayer [34].

In conclusion, based on the experimental data obtained in the current study the primary antibacterial mechanism of action of GN-2 and GN-6 is associated with membrane permeabilization at high peptide concentrations with different kinetics and potencies. At more moderate peptide concentrations it appears that the peptides affect on metabolic disturbance, and further work is required to strengthen these observations.

Acknowledgements

This work was in part funded by The Danish Council for Independent Research (grant # 10-085287). We also acknowledge Professor Lars Holm Øgendal (Niels Bohr Institute, Copenhagen University) for

dynamic light scattering measurements of our liposomes, and Jacob Krake (Roskilde University) for LC-MS analysis.

References

1. Nathan, C., Antibiotics at the crossroads. *Nature* **2004,** *431* (7011), 899-902.
2. von Nussbaum, F.; Brands, M.; Hinzen, B.; Weigand, S.; Habich, D., Antibacterial natural products in medicinal chemistry--exodus or revival? *Angew Chem Int Ed Engl* **2006,** *45* (31), 5072-129.
3. Klevens, R. M.; Morrison, M. A.; Nadle, J.; Petit, S.; Gershman, K.; Ray, S.; Harrison, L. H.; Lynfield, R.; Dumyati, G.; Townes, J. M.; Craig, A. S.; Zell, E. R.; Fosheim, G. E.; McDougal, L. K.; Carey, R. B.; Fridkin, S. K., Invasive methicillin-resistant Staphylococcus aureus infections in the United States. *JAMA* **2007,** *298* (15), 1763-71.
4. Fischbach, M. A.; Walsh, C. T., Antibiotics for emerging pathogens. *Science* **2009,** *325* (5944), 1089-93.
5. Jenssen, H.; Hamill, P.; Hancock, R. E., Peptide antimicrobial agents. *Clin Microbiol Rev* **2006,** *19* (3), 491-511.
6. Hamill, P.; Brown, K.; Jenssen, H.; Hancock, R. E., Novel anti-infectives: is host defence the answer? *Curr Opin Biotechnol* **2008,** *19* (6), 628-36.
7. Hale, J. D.; Hancock, R. E., Alternative mechanisms of action of cationic antimicrobial peptides on bacteria. *Expert Rev Anti Infect Ther* **2007,** *5* (6), 951-9.
8. Jenssen, H.; Hancock, R. E., Antimicrobial properties of lactoferrin. *Biochimie* **2009,** *91* (1), 19-29.
9. Wang, G.; Li, X.; Wang, Z., APD2: the updated antimicrobial peptide database and its application in peptide design. *Nucleic Acids Res* **2009,** *37* (Database issue), D933-7.
10. Fjell, C. D.; Jenssen, H.; Hilpert, K.; Cheung, W. A.; Pante, N.; Hancock, R. E.; Cherkasov, A., Identification of novel antibacterial peptides by chemoinformatics and machine learning. *J Med Chem* **2009,** *52* (7), 2006-15.
11. Godballe, T.; Nilsson, L. L.; Petersen, P. D.; Jenssen, H., Antimicrobial beta-peptides and alpha-peptoids. *Chem Biol Drug Des* **2011,** *77* (2), 107-16.
12. Fjell, C. D.; Jenssen, H.; Cheung, W. A.; Hancock, R. E.; Cherkasov, A., Optimization of antibacterial peptides by genetic algorithms and cheminformatics. *Chem Biol Drug Des* **2011,** *77* (1), 48-56.
13. Wiegand, I.; Hilpert, K.; Hancock, R. E., Agar and broth dilution methods to determine the minimal inhibitory concentration (MIC) of antimicrobial substances. *Nat Protoc* **2008,** *3* (2), 163-75.
14. (a) Falla, T. J.; Karunaratne, D. N.; Hancock, R. E. W., Mode of action of the antimicrobial peptide indolicidin. *Journal of Biological Chemistry* **1996,** *271* (32), 19298-19303; (b) Selsted, M. E.; Novotny, M. J.; Morris, W. L.; Tang, Y. Q.; Smith, W.; Cullor, J. S., Indolicidin, a novel bactericidal tridecapeptide amide from neutrophils. *The Journal of biological chemistry* **1992,** *267* (7), 4292-5.
15. Shai, Y., Mode of action of membrane active antimicrobial peptides. *Biopolymers* **2002,** *66* (4), 236-48.
16. Russell, A. L.; Kennedy, A. M.; Spuches, A. M.; Venugopal, D.; Bhonsle, J. B.; Hicks, R. P., Spectroscopic and thermodynamic evidence for antimicrobial peptide membrane selectivity. *Chem Phys Lipids* **2010,** *163* (6), 488-97.
17. Greenfield, N. J., Using circular dichroism spectra to estimate protein secondary structure. *Nat Protoc* **2006,** *1* (6), 2876-90.
18. Whitmore, L.; Wallace, B. A., Protein secondary structure analyses from circular dichroism spectroscopy: methods and reference databases. *Biopolymers* **2008,** *89* (5), 392-400.

19. (a) Bechinger, B., Structure and functions of channel-forming peptides: magainins, cecropins, melittin and alamethicin. *The Journal of membrane biology* **1997,** *156* (3), 197-211; (b) Brogden, K. A., Antimicrobial peptides: pore formers or metabolic inhibitors in bacteria? *Nature reviews. Microbiology* **2005,** *3* (3), 238-50; (c) Wessman, P.; Stromstedt, A. A.; Malmsten, M.; Edwards, K., Melittin-lipid bilayer interactions and the role of cholesterol. *Biophysical journal* **2008,** *95* (9), 4324-36.
20. (a) Chan, D. I.; Prenner, E. J.; Vogel, H. J., Tryptophan- and arginine-rich antimicrobial peptides: structures and mechanisms of action. *Biochimica et biophysica acta* **2006,** *1758* (9), 1184-202; (b) Schibli, D. J.; Epand, R. F.; Vogel, H. J.; Epand, R. M., Tryptophan-rich antimicrobial peptides: comparative properties and membrane interactions. *Biochem Cell Biol* **2002,** *80* (5), 667-77.
21. Wadhwani, P.; Epand, R. F.; Heidenreich, N.; Burck, J.; Ulrich, A. S.; Epand, R. M., Membrane-active peptides and the clustering of anionic lipids. *Biophysical journal* **2012,** *103* (2), 265-74.
22. Chen, Y.; Guarnieri, M. T.; Vasil, A. I.; Vasil, M. L.; Mant, C. T.; Hodges, R. S., Role of peptide hydrophobicity in the mechanism of action of alpha-helical antimicrobial peptides. *Antimicrobial agents and chemotherapy* **2007,** 51 (4), 1398-406.
23. Slaninova, J.; Mlsova, V.; Kroupova, H.; Alan, L.; Tumova, T.; Monincova, L.; Borovickova, L.; Fucik, V.; Cerovsky, V., Toxicity study of antimicrobial peptides from wild bee venom and their analogs toward mammalian normal and cancer cells. Peptides 2012, 33 (1), 18-26.
24. Eliassen, L. T.; Berge, G.; Leknessund, A.; Wikman, M.; Lindin, I.; Lokke, C.; Ponthan, F.; Johnsen, J. I.; Sveinbjornsson, B.; Kogner, P.; Flaegstad, T.; Rekdal, O., The antimicrobial peptide, lactoferricin B, is cytotoxic to neuroblastoma cells in vitro and inhibits xenograft growth in vivo. International journal of cancer. Journal international du cancer 2006, 119 (3), 493-500.
25. Steen, H. B., Flow cytometry of bacteria: glimpses from the past with a view to the future. J Microbiol Methods 2000, 42 (1), 65-74.
26. Pasotti, L.; Zucca, S.; Lupotto, M.; Cusella De Angelis, M. G.; Magni, P., Characterization of a synthetic bacterial self-destruction device for programmed cell death and for recombinant proteins release. Journal of biological engineering 2011, 5, 8.
27. Walberg, M.; Gaustad, P.; Steen, H. B., Rapid assessment of ceftazidime, ciprofloxacin, and gentamicin susceptibility in exponentially-growing E. coli cells by means of flow cytometry. Cytometry 1997, 27 (2), 169-78.
28. Kohanski, M. A.; Dwyer, D. J.; Collins, J. J., How antibiotics kill bacteria: from targets to networks. Nature reviews. Microbiology 2010, 8 (6), 423-35.
29. Galhardo, R. S.; Hastings, P. J.; Rosenberg, S. M., Mutation as a stress response and the regulation of evolvability. Critical reviews in biochemistry and molecular biology 2007, 42 (5), 399-435.
30. Moussa, M.; Perrier-Cornet, J. M.; Gervais, P., Damage in Escherichia coli cells treated with a combination of high hydrostatic pressure and subzero temperature. Appl Environ Microbiol 2007, 73 (20), 6508-18.
31. Stocks, S. M., Mechanism and use of the commercially available viability stain, BacLight. Cytometry A 2004, 61 (2), 189-95.
32. Huang, H. W., Molecular mechanism of antimicrobial peptides: the origin of cooperativity. Biochimica et biophysica acta 2006, 1758 (9), 1292-302.
33. Spindler, E. C.; Hale, J. D.; Giddings, T. H., Jr.; Hancock, R. E.; Gill, R. T., Deciphering the mode of action of the synthetic antimicrobial peptide Bac8c. Antimicrobial agents and chemotherapy 2011, 55 (4), 1706-16.
34. Hugonin, L.; Vukojevic, V.; Bakalkin, G.; Graslund, A., Membrane leakage induced by dynorphins. FEBS letters 2006, 580 (13), 3201-5.
35. Arbuzova, A.; Schwarz, G., Pore-forming action of mastoparan peptides on liposomes: a quantitative analysis. Biochimica et biophysica acta 1999, 1420 (1-2), 139-52.

36. (a) Irudayam, S. J.; Berkowitz, M. L., Influence of the arrangement and secondary structure of melittin peptides on the formation and stability of toroidal pores. Biochimica et biophysica acta 2011, 1808 (9), 2258-66; (b) Sengupta, D.; Leontiadou, H.; Mark, A. E.; Marrink, S. J., Toroidal pores formed by antimicrobial peptides show significant disorder. Biochim Biophys Acta 2008, 1778 (10), 2308-17.
37. Allende, D.; Simon, S. A.; McIntosh, T. J., Melittin-induced bilayer leakage depends on lipid material properties: evidence for toroidal pores. Biophysical journal 2005, 88 (3), 1828-37.
38. Rex, S.; Schwarz, G., Quantitative studies on the melittin-induced leakage mechanism of lipid vesicles. Biochemistry 1998, 37 (8), 2336-45.
39. (a) Pistolesi, S.; Pogni, R.; Feix, J. B., Membrane insertion and bilayer perturbation by antimicrobial peptide CM15. Biophys J 2007, 93 (5), 1651-60; (b) Teixeira, V.; Feio, M. J.; Bastos, M., Role of lipids in the interaction of antimicrobial peptides with membranes. Progress in lipid research 2012, 51 (2), 149-77.

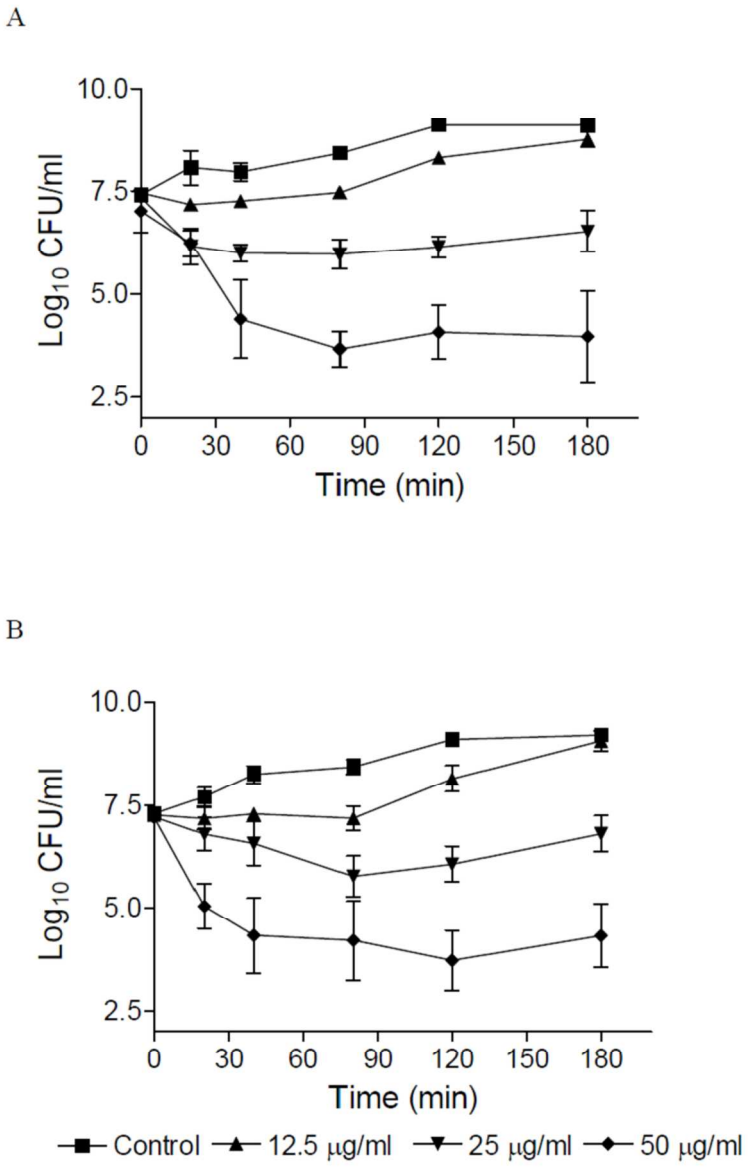

Figure 1. Viability of exponentially growing E. coli ATCC 25922 exposed to 1x, 2x, and 4x MIC concentrations of (A) GN-2 peptide and (B) GN-6 peptide over a course of 3 hours. Data represent mean and SEM of 3 independent experiments.
97x148mm (600 x 600 DPI)

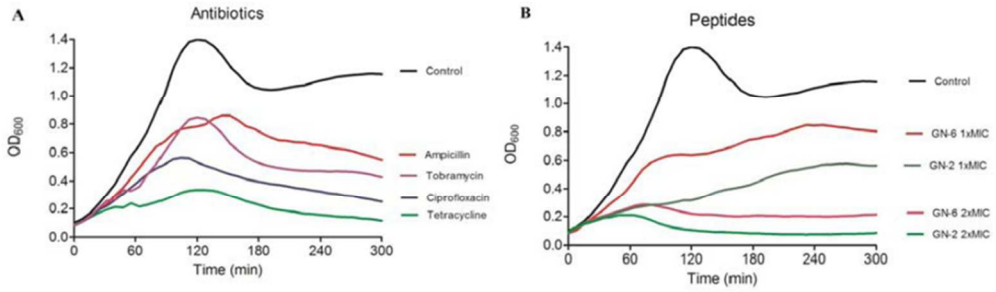

Figure 2. Optical density measurements of exponentially growing E. coli ATCC 25922 over 5 hours. Data presents mean of 3 independent experiments based. Bacterial growth at 37°C in a 96-well plates from a starting inoculum of OD600 of 0.1 has been measured with 8 minutes intervals. (A) Bacteria exposed to antibiotics at MIC concentrations, Ampicillin (4 µg/ml), Tobramycin (0.78 µg/ml), Tetracycline (1 µg/ml) and Ciprofloxacin (0.05 µg/ml). (B) Bacteria exposed to GN-2 peptide at 1x MIC (6.2 µg/ml) and 2x MIC (12.5 µg/ml) and GN-6 peptide at 1x MIC (12.5 µg/ml) and 2x MIC (25 µg/ml) concentrations.
42x12mm (600 x 600 DPI)

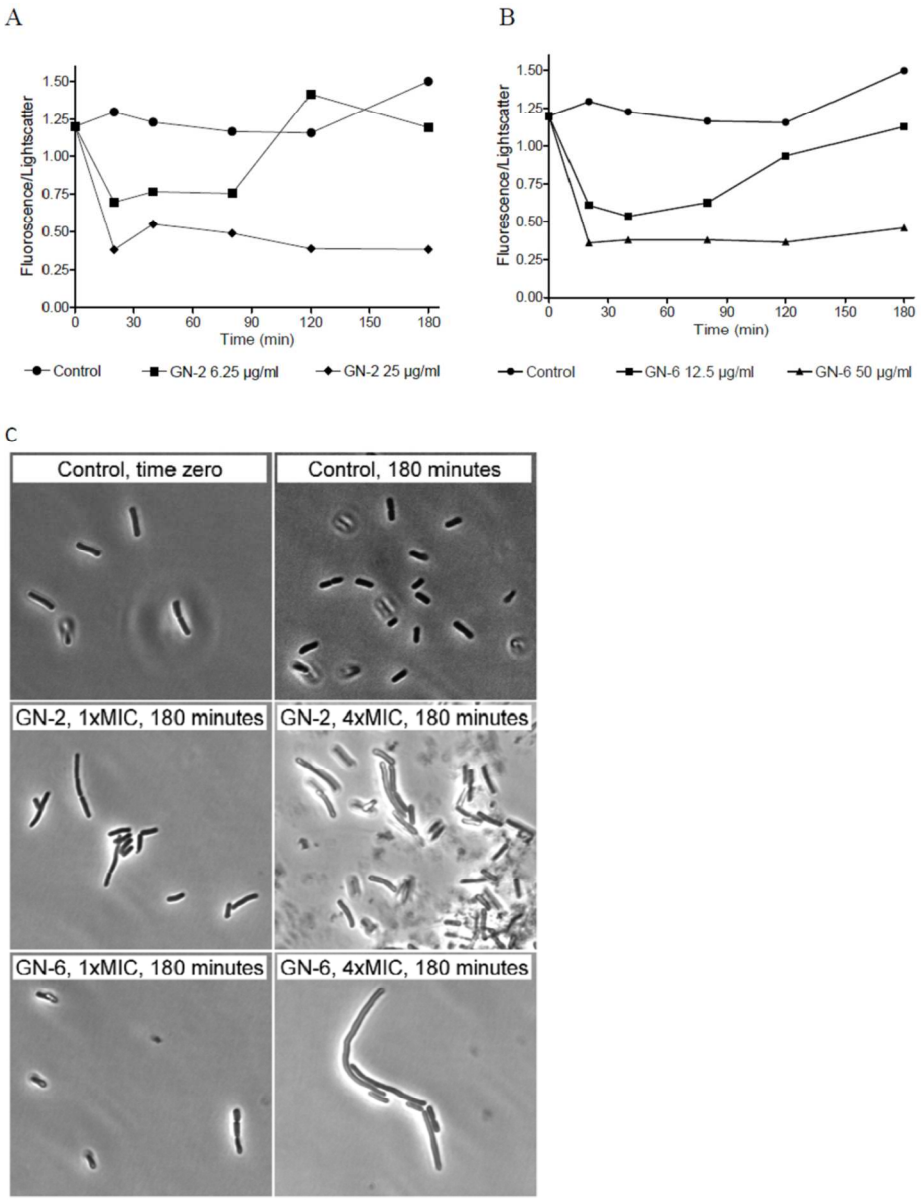

Figure 3. Peptide effect on E. coli morphology. (A,B) Flow cytometry data of GN-2 and GN-6 peptide influence on the DNA content per cell mass represented by fluorescence/lightscatter ratio, respectively. Data collected over a course of 3 hours in a microtitter plate format with an inoculum of OD600 of 0.1 and incubated at 37°C between extractions. (C) Microscope images of ethanol stained flow cytometry samples of E. coli treated with GN-2 and GN-6 peptide at 1x and 4xMIC concentration for 3 hours. Bacteria without cellular content appear transparent. Pictures taken at same magnification with a Leica DM5000 B microscope.
87x113mm (600 x 600 DPI)

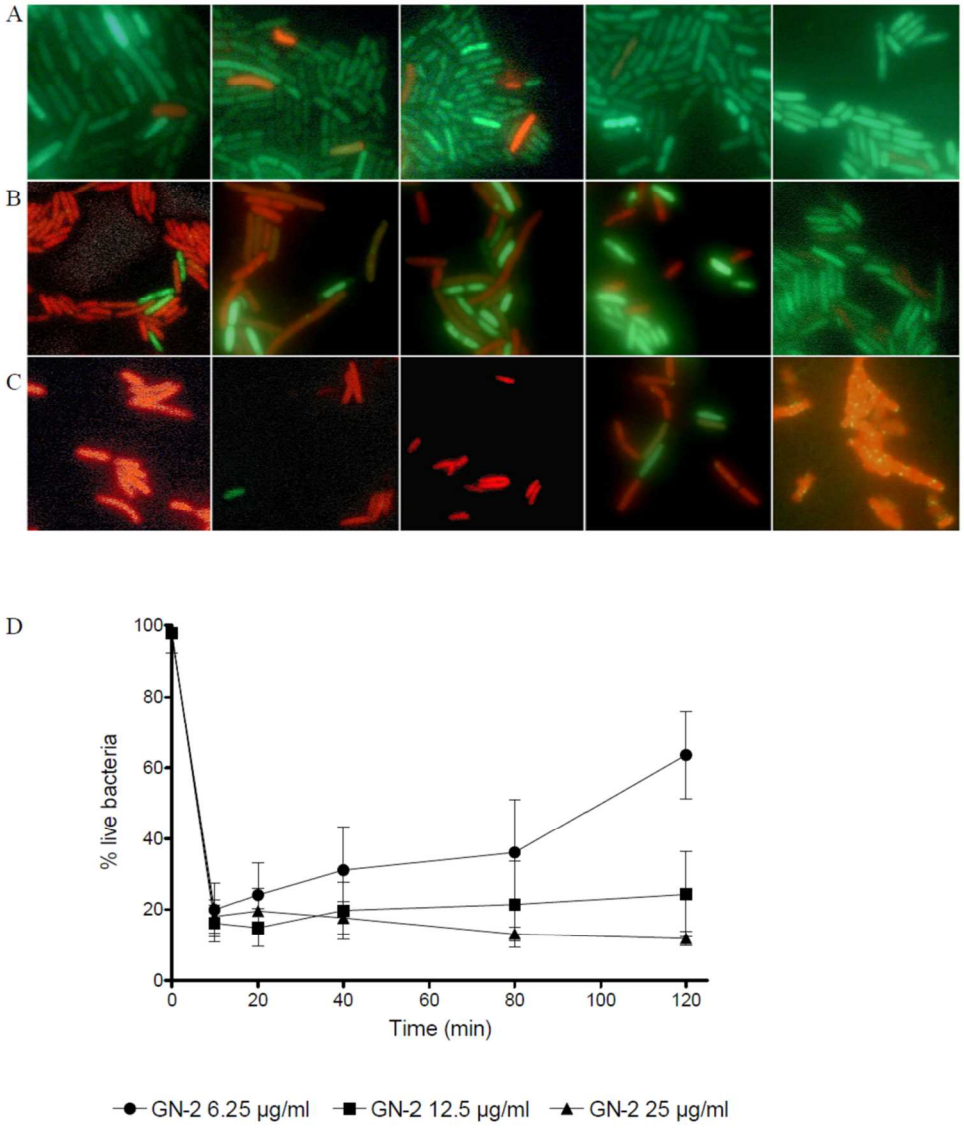

Figure 4. Visualization and quantification of membrane permeabilization of GN-2 peptide on E. coli ATCC 25922 over a period of 120 minutes. (A) Control cells. (B) Bacteria exposed to 1xMIC GN-2 peptide. (C) Bacteria exposed to 4xMIC GN-2 peptide. (D) Percentage of live bacteria after treatment with 1x, 2x and 4xMIC concentration of peptide GN-2. Pictures taken with Leica DM5000B microscope using mercury lamp. 118x138mm (600 x 600 DPI)

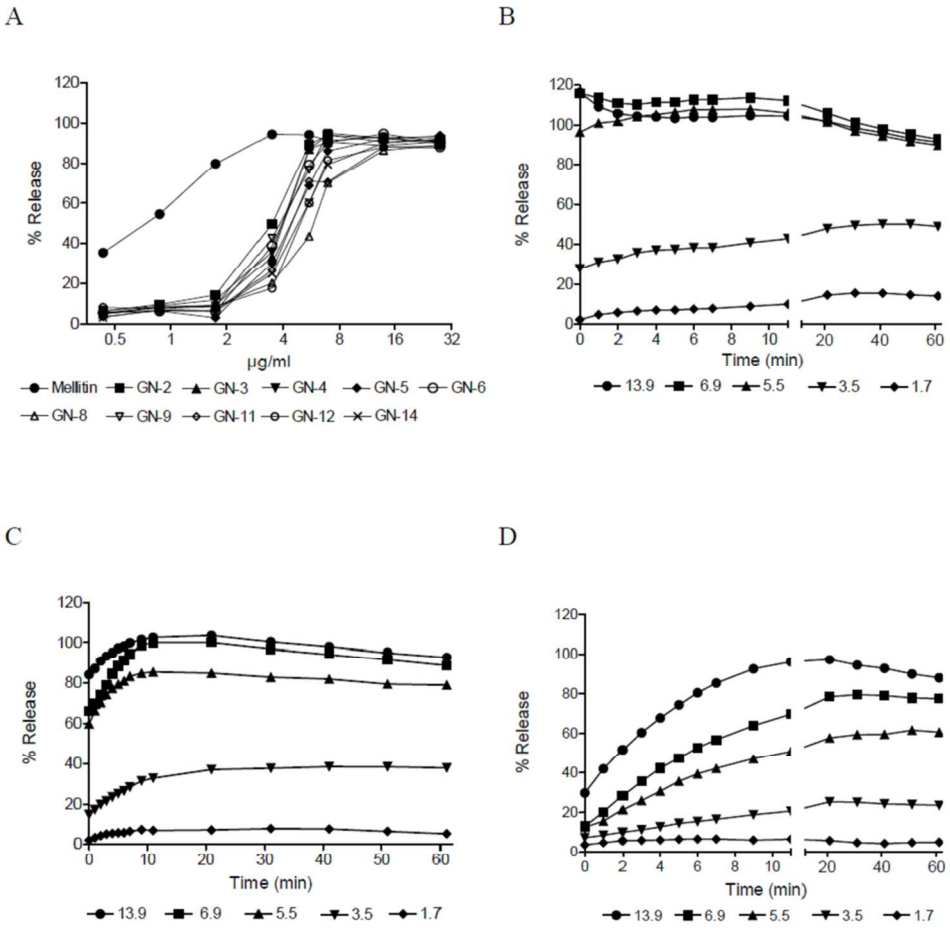

Figure 5. Calcein release from POPG:POPC vesicles. (A) Calcein leakage measurements from 20 µM POPG:POPC (7:3) vesicles at 37°C at various peptide concentrations in a 96-well format assay at 60 min. All readings are baseline corrected by subtracting values from wells containing only liposomes. 100% leakage is estimated as a total calcein release from liposomes exposed to 10 % Triton X-100. Represented results are mean values of three independent experiments with good reproducibility. Standard error bars are omitted for clarity. Calcein leakage measurements from 20 µM POPG:POPC (7:3) vesicles at 37°C at various concentrations of (B) GN-2, (C) GN-6 and (D) GN-14, in a 96-well format assay over a period of 1 hour. 76x74mm (600 x 600 DPI)

Table 1. Peptide characteristics, antimicrobial activity and toxicity

Peptide	Sequence	HPLC retention-time (min)	Hydrophobic moment	Minimal Inhibitory Concentration (µg/ml)			< 10 % Hemolysis	IC50
				E. coli	*P. aeruginosa*	*S. aureus*		
GN-2	RWKRWWRWI-$CONH_2$	6.33	5.4	6.2	3.1	3.1	100	47
GN-3	KWWRWRRWW-$CONH_2$	6.62	3.3	12.5	25	6.2	100	106
GN-4	RWKKWWRWL-$CONH_2$	6.54	5.5	6.2	3.1	6.2	100	37
GN-5	KKRWWWWWR-$CONH_2$	7.10	2.8	12.5	6.2	1.5	100	131
GN-6	RKRWWWWFR-$CONH_2$	7.08	2.8	12.5	6.2	3.1	100	97
GN-8	IWKRWWWKR-$CONH_2$	4.54	2.2	25	100	50	> 400	199
GN-9	RIWKIWWKR-$CONH_2$	4.63	4.8	25	25	> 50	> 400	> 200
GN-11	IKWKRWWWR-$CONH_2$	5.88	3.4	12.5	50	25	> 400	> 200
GN-12	KWWKIWRWR-$CONH_2$	6.13	2.9	25	12.5	12.5	> 400	173
GN-14	RLWKRWWIR-$CONH_2$	4.43	4.4	6.2	100	25	100	> 200
Indolicidin	ILPWKWPWWPWRR-$CONH_2$	ND	1.2	25	100	12.5	100	> 200

Table 1: Hydrophobic moment is a quantitative measure of amphipathicity calculated with HydroMCalc using the CCS scale. Median MIC values of GN peptides in µg/ml against *E. coli* ATCC 25922, *P. aureginosa* PA01 and *S. aureus* ATCC 29213 obtained by 3 repeated experiments. Hemolysis values are the mean concentration in µg/ml recorded over 3 experiments that induced less than 10% hemolysis. IC50 values in µg/ml is a toxicity measurement resulting from the MTT assays performed on HeLa cells, and calculated from the equation Y=Bottom + (Top-Bottom)/(1+10^((LogIC50-X)*HillSlope)).

Figure 1. Viability of exponentially growing *E. coli* ATCC 25922 exposed to 1x, 2x, and 4x MIC concentrations of (**A**) GN-2 peptide and (**B**) GN-6 peptide over a course of 3 hours. Data represent mean and SEM of 3 independent experiments.

Figure 2. Optical density measurements of exponentially growing *E. coli* ATCC 25922 over 5 hours. Data presents mean of 3 independent experiments based. Bacterial growth at 37°C in a 96-well plates from a starting inoculum of OD_{600} of 0.1 has been measured with 8 minutes intervals. (**A**) Bacteria exposed to antibiotics at MIC concentrations, Ampicillin (4 μg/ml), Tobramycin (0.78 μg/ml), Tetracycline (1 μg/ml) and Ciprofloxacin (0.05 μg/ml). (**B**) Bacteria exposed to GN-2 peptide at 1x MIC (6.2 μg/ml) and 2x MIC (12.5 μg/ml) and GN-6 peptide at 1x MIC (12.5 μg/ml) and 2x MIC (25 μg/ml) concentrations.

Figure 3. Peptide effect on *E. coli* morphology. (**A,B**) Flow cytometry data of GN-2 and GN-6 peptide influence on the DNA content per cell mass represented by fluorescence/lightscatter ratio, respectively. Data collected over a course of 3 hours in a microtitter plate format with an inoculum of OD_{600} of 0.1 and incubated at 37°C between extractions. (**C**) Microscope images of ethanol stained flow cytometry samples of *E. coli* treated with GN-2 and GN-6 peptide at 1x and 4xMIC concentration for 3 hours. Bacteria without cellular content appear transparent. Pictures taken at same magnification with a Leica DM5000 B microscope.

Figure 4. Visualization and quantification of membrane permeabilization of GN-2 peptide on *E. coli* ATCC 25922 over a period of 120 minutes. (**A**) Control cells. (**B**) Bacteria exposed to 1xMIC GN-2 peptide. (**C**) Bacteria exposed to 4xMIC GN-2 peptide. (**D**) Percentage of live bacteria after treatment with 1x, 2x and 4xMIC concentration of peptide GN-2. Pictures taken with Leica DM5000B microscope using mercury lamp.

Figure 5. Calcein release from POPG:POPC vesicles. (**A**) Calcein leakage measurements from 20 μM POPG:POPC (7:3) vesicles at 37°C at various peptide concentrations in a 96-well format assay at 60 min. All readings are baseline corrected by subtracting values from wells containing only liposomes. 100% leakage is estimated as a total calcein release from liposomes exposed to 10 % Triton X-100. Represented results are mean values of three independent experiments with good reproducibility. Standard error bars are omitted for clarity. Calcein leakage measurements from 20

μM POPG:POPC (7:3) vesicles at 37°C at various concentrations of (**B**) GN-2, (**C**) GN-6 and (**D**) GN-14, in a 96-well format assay over a period of 1 hour.